†V included in NiVTi$_2$S$_4$ represents "vacancy."
[1]S. Anzai and K. Ozawa, J. Phys. Soc. Jap. **24**, 271 (1968).
[2]J. T. Sparks and T. Komoto, Phys. Lett. A **25**, 398 (1967).
[3]J. M. Tyler and J. L. Fry, Phys. Rev. B 1, 4604 (1970).
[4]R. M. White and N. F. Mott, Philos. Mag. **24**, 845 (1971).
[5]R. H. Plovnick, D. S. Perloff, M. Vlasse, and A. Wold, J. Phys. Chem. Solids **29**, 1935 (1968).
[6]C. P. Bean and D. S. Rodbell, Phys. Rev. **126**, 104 (1962).
[7]L. A. Girifalco and V. G. Weizer, Phys. Rev. **114**, 687 (1959).
[8]N. F. Mott, Proc. Phys. Soc. Lond. **49**, 258 (1937).
[9]K. Ozawa and S. Anzai, Phys. Status Solidi **17**, 697 (1966).
[10]B. L. Morris, R. H. Plovnick, and A. Wold, Solid State Commun. **7**, 291 (1969).
[11]H. Sato and R. S. Toth, Phys. Rev. **124**, 1833 (1961).
[12]S. L. Holt, R. J. Bouchard, and A. Wold, J. Phys. Chem. Solids **27**, 755 (1966).
[13]R. J. Bouchard and A. Wold, J. Phys. Chem. Solids **27**, 591 (1966).
[14]M. Sachs, *Solid State Theory* (McGraw-Hill, New York, 1963), p. 297.
[15]L. Pauling, *The Nature of the Chemical Bond* (Cornell U. P., New York, 1960), p. 93.
[16]D. N. Yoon and A. Bienenstock, Phys. Rev. **170**, 631 (1968).
[17]D. N. Yoon and R. N. Jeffery, J. Phys. Chem. Solids **31**, 2635 (1970).

PHYSICAL REVIEW B VOLUME 7, NUMBER 7 1 APRIL 1973

Lattice Modes in Ferroelectric Perovskites: $PbTiO_3$ †

Gerald Burns and Bruce A. Scott
IBM Thomas J. Watson Research Center, Yorktown Heights, New York 10598
(Received 12 June 1972)

A complete study of the lattice-dynamical behavior of the ferroelectric tetragonal perovskite $PbTiO_3$ has been carried out using Raman spectroscopy. The temperature dependence of all the long-wavelength mode frequencies are determined. We show that a damped-harmonic-oscillator model with a frequency-independent damping coefficient is sufficient to explain the observed shape of the soft E(1TO) mode in the ferroelectric phase at all temperatures below $T_c = 493$ °C. Moreover, by combining our experimental mode-frequency data with pyroelectric measurements of the change in spontaneous polarization P_s with temperature, we obtain values of $P_s(25\,°C) = 81\ \mu C/cm^2$ and $P_s(T_c) = 42\ \mu C/cm^2$. This is in excellent agreement with a recent direct experimental measurement. The temperature dependence of all the mode strengths has also been determined to T_c. These results are used to extract the temperature dependence of the clamped dielectric constants. In $PbTiO_3$ the dielectric constant along the ferroelectric axis ϵ_c is determined primarily by the lowest frequency A_1(1TO) mode at all temperatures to T_c, in contrast to $BaTiO_3$ where in the ferroelectric phase the lowest mode determines only $\approx 25\%$ of ϵ_c. In $PbTiO_3$ the dielectric constant perpendicular to the c axis ϵ_a is also determined by the lowest E(1TO) mode at all temperatures. The possibility of observing critical effects near T_c in the soft-mode data of $PbTiO_3$ has been examined. These effects are not observed. Also, it is shown that very careful fitting of the soft-mode temperature dependence to a functional form containing a minimum number of separately determined parameters is required before critical effects can be invoked in first-order phase transitions of the displacive type.

I. INTRODUCTION

A large number of ABO_3 compounds having the perovskite structure (Fig. 1) display ferroelectric or other types of structural phase transitions.[1] From the point of view of both physical properties and device applications, the literature on the perovskite $BaTiO_3$ is especially extensive.[1,2] For these reasons, $BaTiO_3$ was one of the first perovskite ferroelectrics to be studied when the first suggestions appeared in the literature concerning the role played by lattice dynamics in the displacive ferroelectric phase transition.[3] Since that time it has become clear that $BaTiO_3$ is not an ideal displacive ferroelectric.[4-7] For example, the predicted connection, through the Lydanne–Sachs–Teller (LST) relationship, between lattice dynamics and the temperature-dependent, damped low-frequency dielectric constant $\epsilon(0)$ was observed not in $BaTiO_3$, but in $SrTiO_3$[8,9] and $KTaO_3$[10,11] perovskites. These crystals never undergo the ferroelectric transition although $\epsilon(0)$ reaches large values at temperatures approaching 0 °K in both these materials. More recently, Raman,[4(c),4(d),12,13] infrared,[5] neutron scattering,[14] and x-ray experiments[15] have revealed that $BaTiO_3$ does not behave ideally because the "soft" optic mode responsible for the cubic-to-tetragonal ferroelectric phase transition is highly overdamped. Preliminary Raman studies[16] of $KNbO_3$ suggest similar behavior.

Against the background just described, it was interesting to discover that the ferroelectric perovskite $PbTiO_3$ behaves in the expected manner; in fact, it appears to be a textbook example of a displacive ferroelectric phase transition. The Raman measurements[17] show that (a) selection

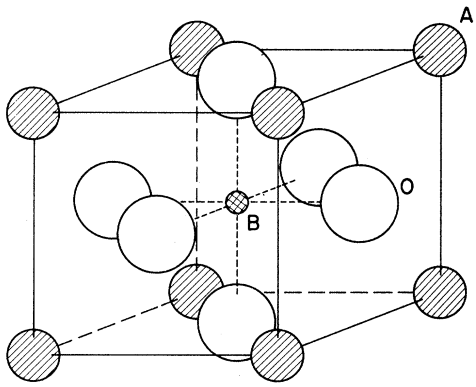

FIG. 1. Cubic ABO_3 perovskite structure.

rules below the transition temperature T_c in the tetragonal ferroelectric phase are obeyed for all the modes, (b) the modes are sharp and underdamped below T_c, and (c) the modes abruptly disappear above T_c as expected from the selection rules. The neutron results[18] for $PbTiO_3$ also show well-behaved modes. Above T_c the lowest mode is underdamped throughout the Brillouin zone except for very small wave vectors, and the lowest optic modes at room temperature also are underdamped.[1]

In the present paper, we extend our earlier Raman studies of the ferroelectric $PbTiO_3$ in several ways. Using exact expressions, instead of the electrostatic approximation,[19] for the angular dependence of the "quasimode" spectra, we present the temperature dependences of all the mode frequencies. We show that for $PbTiO_3$ a damped-harmonic-oscillator model with a frequency-independent damping constant is sufficient to explain the observed line shapes. Also, we use a series of empirical fitting procedures combined with experimental mode-frequency data to obtain the polarization-vs-temperature relationship for $PbTiO_3$, and mode strength data to obtain the temperature dependence of the true clamped dielectric constants. These results are further compared with those predicted from the Devonshire free-energy formulation, and comparisons made with $BaTiO_3$. The results will also be compared to the unpolarized Raman data.[20]

II. EXPERIMENTAL

Crystals of $PbTiO_3$ used in this work were grown by the flux technique using the phase equilibrium data obtained by Sholokhovich in the PbO-TiO_2-B_2O_3 system.[21] The melts utilized were comprised of compositions in the range 50–70-mole% PbO, 25–15-mole% TiO_2 and 25–15%-mole% B_2O_3. The melts, contained in covered 100-cc platinum crucibles, were placed into a furnace having a vertical temperature gradient of 5 °C/in. at 1150 °C, held for 2 h, and then program cooled at a rate of 3 °C/hr to 800 °C. At this temperature the liquid was decanted, and the crucible cooled under thermal insulation to room temperature (~8 h). It was found that melts containing the greater PbO content (approaching 70 mole%) yielded thin crystal platelets of large area (5×5×0.5 mm), whereas increasing the TiO_2 and B_2O_3 content in the melts resulted in long rectangular parallelpipeds (~1×1×5 mm). Some of the latter crystals showed single-domain regions of excellent optical quality. These were used for the Raman experiments. It proved impossible to pole the multidomain crystals due to the high conductivity of the samples above 300 °C. Apparently, U^{3+} doping of the crystals increases the resistivity enough to permit measurement of the dielectric constant to above the transition temperature.[22] However, the crystals used here were undoped.

The Raman measurements were obtained using a conventional apparatus. A Spectra Physics 140 He-Ne laser with an output of approximately 70 mW at 6328.2 Å was used. The argon laser was not used on the $PbTiO_3$ crystals because they became rapidly discolored by the laser presumably from local heating. (The crystals had a slight yellow-green color.) The collected right-angle-Raman-scattered light was focused into the entrance slit of a Jarrel–Ash double monochrometer (with gratings blazed at 5500 Å) and detected with a small-area FW-130 photomultiplier. The current from the photomultiplier was measured with a microammeter (HP425A) and displayed on a chart recorder.

The sample was mounted in a temperature-controlled furnace constructed from silver, for good conduction, and Lavite for insulation, as shown in Fig. 2. It was heated with a small Hotwatt heater (Hotwatt Corp., Danvers, Mass.) and was used to 620 °C. The furnace was found to be very convenient for Raman measurements. It permits sample mounting and measurement at room temperature before putting on the furnace top.

III. FREQUENCIES OF VIBRATIONAL MODES AND ANGULAR DEPENDENCE

The space group is O_h^1, with one formula unit per cell, in the high-temperature cubic phase of $PbTiO_3$. Thus there are $(3n-3)=12$ optic modes at long wavelength, or wave vector $k \approx 0$ ($k = 2\pi/\lambda$). The optic modes transform as the $3T_{1u}+T_{2u}$ irreducible representation of the point group O_h. The T_{2u} "silent mode" is triply degenerate and not Raman or infrared active. The three triply degenerate T_{1u} modes are infrared active; i.e., an oscillating dipole moment or polarization is associated with the mode displacements. The long-range electrostatic forces lift the degeneracy for

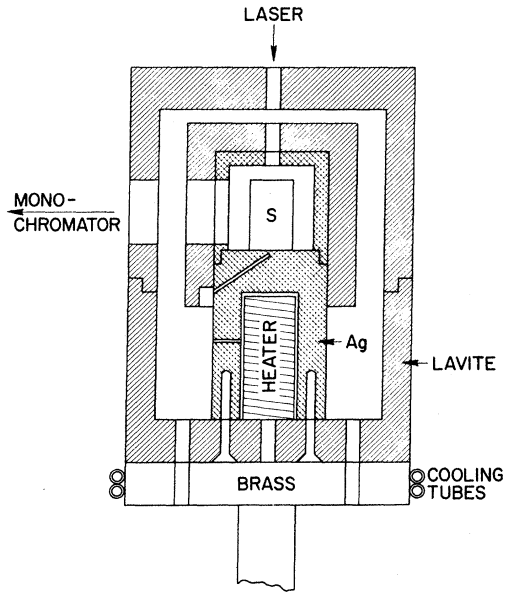

FIG. 2. Furnace arrangement for Raman spectroscopy to 620 °C. (*S* is the sample.)

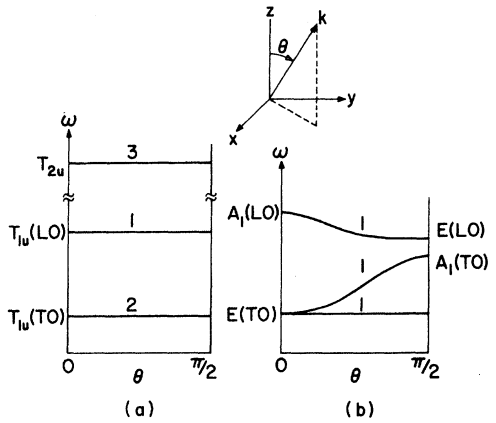

FIG. 3. Frequencies of the transverse optic (TO) and longitudinal optic (LO) modes as a function of θ, the angle between the c axis and phonon vector $\vec{k}$. (a) Cubic O_h case; (b) tetragonal C_{4v} case.

$k \approx 0$ vibrations into a doubly degenerate transverse mode T_{1u}(TO) with polarization perpendicular to $\vec{k}$, and a single longitudinal mode T_{1u}(LO) with polarization parallel to $\vec{k}$. Figure 3(a) shows a dependence of the frequencies of these modes on θ, the angle between $\vec{k}$ and the c axis of the crystal. (The polar c axis is derived from one of the three cubic axes. The c axis is taken as the direction of the spontaneous polarization in the tetragonal ferroelectric phase.) In the ferroelectric tetragonal phase (C_{4v}^1 space group) each cubic T_{1u} mode transforms as the $A_1 + E$ irreducible representation of C_{4v}. Figure 3(b) conceptually shows the behavior of the mode frequencies vs θ. The usual group-theoretical labeling is included for $\theta = 0$ and $\frac{1}{2}\pi$. It is only when $\vec{k}$ is along these principal directions that all the modes can be exactly described by the irreducible representation of C_{4v}. The modes are termed quasimodes or oblique phonons at intermediate values of θ.

When frequencies of normal modes are quoted, the values given are always for normal modes along principal crystalline directions. For a tetragonal crystal, as discussed here, these are the frequencies for $\theta = 0$ and $\frac{1}{2}\pi$. In the tetragonal phase the cubic T_{2u} silent mode will transform as the $B_1 + E$ irreducible representation of C_{4v}. Thus, in principle, the degeneracy of this mode will be removed. However, such a splitting has not experimentally been observed in this work at any value of θ. We continue to call this mode the "silent" mode even in the C_{4v} phase, where it is infrared and Raman active. This nomenclature will be used since it permits clearer labeling of the other modes. The other modes that arise from the $3T_{1u}$ cubic modes can then be labeled in sequence 1, 2, and 3. For example, the three E(TO) modes will be called E(1TO), E(2TO), and E(3TO) as will be done for the $3A_1$(TO), $3A_1$(LO), and $3E$(LO).

We proceed now to describe the results of our measurements of the mode frequencies. Figure 4 shows the temperature dependence of all of the allowed modes below T_c. All of the TO modes were measured directly except the lowest A_1(1TO) mode.

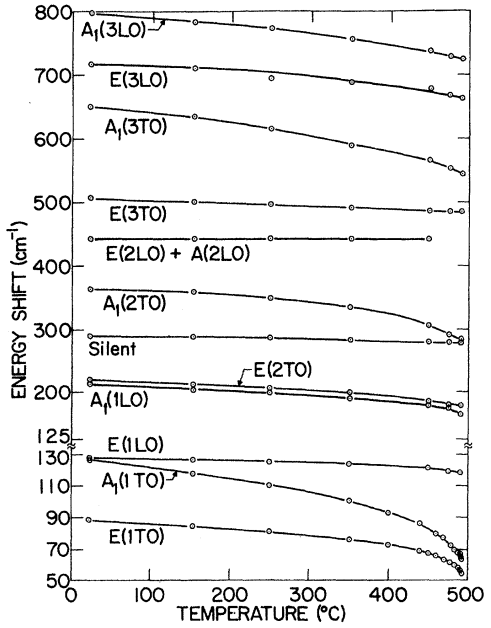

FIG. 4. Experimental results for the temperature dependence of the lattice modes in $PbTiO_3$.

In general, the LO modes were weaker. These were directly measured except $A_1(1\mathrm{LO})$ and $E(3\mathrm{LO})$. The specific directions and polarizations used are given in Ref. 17. Basically, specific crystal orientations are used so that $\vec{k}$ can be along various principal axes of the crystal. Then the polarization of the input and scattered light is adjusted so that A_1 or E modes are measured. For the right-angle scattering measurements carried out in the present work, $\vec{k}$ is at 45° to incident and scattered directions ($\vec{k}_i = \vec{k}_s + \vec{k}$) and $k_i \approx k_s$. Thus, some of the modes must be measured by directing the incident light along the $x+z$ direction, and measuring the light scattered along the x-z directions, etc.[17] In Ref. 17 the frequencies of the modes that could not be directly measured were determined from the quasimode spectrum at $\theta = 45°$ using the electrostatic approximation.[19] Figure 4 shows somewhat different results than Ref. 17 for these modes because here Merten's[19,23] exact expressions were used to relate the $\theta = 45°$ data to the principal-axis modes.

We now describe Merten's equation and compare results obtained with it to those obtained with the electrostatic approximation. In a uniaxial crystal having symmetry such as C_{4v}, the dielectric constant as a function of frequency and θ is given by[23]

$$\epsilon_c(\omega)\cos^2\theta + \epsilon_a(\omega)\sin^2\theta = 0\,, \tag{1}$$

where θ is the angle between $\vec{k}$ and the c axis, $\epsilon_c(\omega)$ is the dielectric constant along the c axis as a function of ω, and $\epsilon_a(\omega)$ is the frequency dependence of ϵ along the a axis. Along any of the principle axis Eq. (1) gives the frequencies of the LO modes, i.e., $\epsilon_c(\omega) = 0$. However, for an arbitrary value of θ all infrared-active modes will have a component of polarization parallel and perpendicular to the propagation direction. Thus, for arbitrary θ this equation applies to all the infrared-active modes, i.e., those that are labeled LO and TO along the principal axes.[23] The dielectric constant along either of the principal axes can be written in terms of the TO and LO frequencies[24]:

$$\frac{\epsilon_c(\omega)}{\epsilon_c(\infty)} = \frac{\prod_i [\omega_c(i\mathrm{LO})^2 - \omega^2]}{\prod_i [\omega_c(i\mathrm{TO})^2 - \omega^2]}\,,$$
$$\frac{\epsilon_a(\omega)}{\epsilon_a(\infty)} = \frac{\prod_i [\omega_a(i\mathrm{LO})^2 - \omega]}{\prod_i [\omega_a(i\mathrm{TO}) - \omega^2]}\,, \tag{2}$$

where ω_c and ω_a are the frequencies of the A_1 and E modes, respectively, and $\epsilon(\infty)$ is the dielectric constant in a frequency region high compared to all the lattice modes, but low compared to the electronic energies. For $\omega = 0$, Eq. (2) gives the familiar Lyddane–Sachs–Teller relationship[3] for the dielectric constant along principal axes. Combining Eq. (2) with Eq. (1) yields

$$\epsilon_c(\infty)\cos^2\theta \prod[\omega_c(i\mathrm{LO})^2 - \omega^2] \prod[\omega_a(i\mathrm{TO})^2 - \omega^2]$$
$$+ \epsilon_a(\infty)\sin^2\theta \prod[\omega_a(i\mathrm{LO})^2 - \omega^2] \prod[\omega_c(i\mathrm{TO})^2 - \omega^2] = 0. \tag{3}$$

This is the usual form of Merten's equation.[23] If all the $3n-3$ optic modes along the principal axis are known, i.e., the frequencies ω_a and ω_c of all the TO and LO phonons, then at any particular value of θ the $3n-3$ values of ω that satisfy Eq. (3) are the frequencies of vibration of the crystal. These normal modes of the crystal at oblique angles are sometimes called mixed symmetry modes, quasimodes, or oblique modes. These modes correspond to a general $\vec{k}$ direction as opposed to $\vec{k}$ along a special direction in the Brillouin zone. As is well known in band theory, for a general point $\vec{k}$ not at a special point or along a special line) all the eigenfunctions transform as the same one-dimensional irreducible representation. Therefore, the eigenfunctions will have different energies and there will be a repulsion of the energy levels.

A trial and error method was used to determine the $3n-3$ values of ω that satisfy Eq. (3) for a given θ. All the solutions must lie between the extreme values of ω_c or ω_a. Figure 5 shows the results for $PbTiO_3$ at 23 °C. These curves were calculated after all the principal-axis modes were determined. As mentioned previously, the $A_1(1\mathrm{TO})$, $A_1(1\mathrm{LO})$, and $E(3\mathrm{LO})$ modes were too weak to determine directly. The frequencies for these prin-

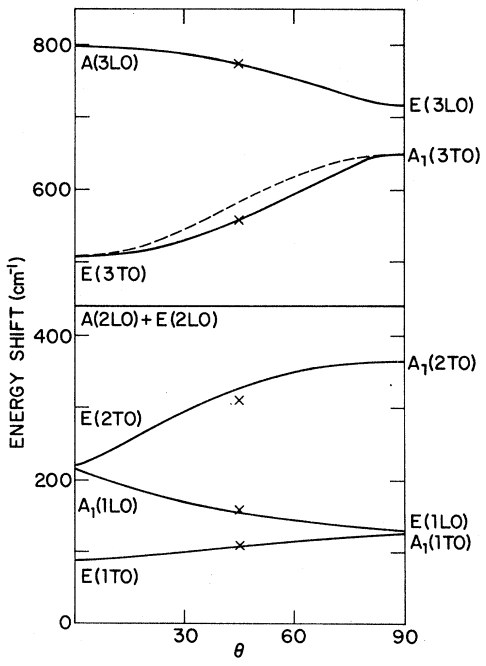

FIG. 5. Frequencies of several A_1 and E modes as a function of θ calculated from Merten's equations (Ref. 23) (solid curves) and the electrostatic approximation (Ref. 19) (dashed curve). The experimental values at $\theta = 45°$C are shown as crosses.

cipal-axis modes first were determined by using Eq. (3), the other principal-axis modes were directly measured, and trial and error was used to find a best fit using the measured quasimodes at $\theta = 45°$, at $\omega = 105$, 159, and 772 cm^{-1}. This procedure was repeated at elevated temperatures to give the results shown in Fig. 4. To test these procedures we compared the results from Eq. (3) to the quasimodes measured at $\theta = 45°$ with the experimentally observed value at $\omega = 310$ and 559 cm^{-1} shown in Fig. 5. The agreement between the measurement and calculation for the quasimode connecting the E(3TO) and A_1(3TO) modes is excellent. This was true at all temperatures. The agreement between calculated and experimental values for the quasimode between E(2TO) and A_1(2TO) modes is less satisfactory. It was initially suspected that this was due to the influence of the silent mode at 292 cm^{-1}. However, as discussed later, the silent-mode strength has been found to be extremely small and should have little effect on the quasimodes.

Figure 5 also shows the results for the electrostatic approximation (dashed curve) for the quasimode connecting the E(3TO) and A_1(3TO) modes. The equation for this curve is[19]

$$\omega^2 = [\omega(A_1(\mathrm{TO}))]^2 \sin^2\theta + [\omega(E(\mathrm{TO}))]^2 \cos^2\theta \ . \quad (4)$$

At $\theta = 45°$ the two curves differ by ≈ 20 cm^{-1}. This difference illustrates the fact that the electrostatic approximation will show reasonable agreement with experiment if the principal-axis modes that occur at $\theta = 0°$ and 90° are not widely separated in frequency. For the case shown here, the principal-axis modes are separated by almost 150 cm^{-1} and the largest difference between the electrostatic approximation and Merten's equation is 20 cm^{-1}. Actually, the difference may be larger as will be shown in the following discussion.

Figure 5 shows an angular dependence in which the E(TO) solutions are always connected to A_1(TO). Similarly, E(LO) and A_1(LO) are connected, but in both cases the results are accidental. In fact, it would appear from Fig. 4 that A_1(1TO) and E(1LO) will cross at lower temperature. It should be appreciated that solutions of Eq. (3) will connect modes of any two symmetries.

Figure 6 shows an example in which the modes at $\theta = 0°$ are fixed, but with two different possibilities for the modes at $\theta = 90°$. In example 1, the figure shows the solutions of Eq. (3), in which an E(TO) mode is connected to an E(LO) mode. This happens because the E(LO) mode is lower in energy than the A_1(TO) mode. Similarly, in example 1 the A_1 modes are connected together. Example 2 shows the E(LO) mode 5 cm^{-1} higher than the A_1(TO). Solutions of Eq. (3) show that the LO modes are connected to each other. Similarly, the

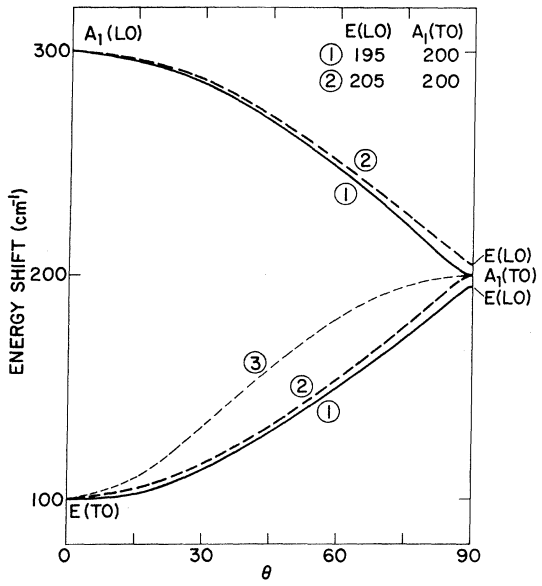

FIG. 6. Three possible connection schemes for TO and LO modes of A_1 and E symmetry. Details of the schemes are given in the text.

TO modes are connected to each other. As discussed above, the no-crossing rule for these general point in $\vec{k}$ space determines the ordering of the levels. Several other points should be observed from Eq. (3) and Fig. 6. For modes along principal directions $d\omega/d\theta = 0$ always holds. This is particularly important for considerations of powder Raman spectra.[25] The strong repulsion of the modes near $\theta = 90°$ can be seen in Fig. 6. Also shown in Fig. 6 is the result for the simple electrostatic approximation, Eq. (4), which connects an E(TO) mode at 100 cm^{-1} to the A_1(TO) mode at 200 cm^{-1} (example 3). The largest separation between curves 2 and 3 is greater than 26 cm^{-1} and occurs for $\theta \simeq 50°$. The large difference between the simplified quasimode solution, Eq. (4), and the general solution, Eq. (3), is due to the repulsion of these particular quasimodes. As can be seen, the error in employing the solutions of Eq. (4) instead of Eq. (3) is 26% for the case illustrated.

IV. LINE SHAPE

There are two important reasons for examining the Raman line shape. First, near T_c the ratio of the linewidth to line position becomes of the order of $\frac{1}{2}$ for the soft E(1TO) mode. Thus, a detailed fit to the shape must be made to properly determine the frequency ω_0 and damping constant γ (generalized linewidth) of the line as a function of temperature. Second, we can examine the frequency dependence of γ, for which there is considerable theoretical interest. The reason this can be done using the $PbTiO_3$ data near T_c is that $\gamma/\omega_0 \approx 27$

$cm^{-1}/54\ cm^{-1}$ so that the Raman response is measurable from $\omega \sim 0$ to 100 cm^{-1}.

The frequency dependence of the dielectric constant can be written as a sum of damped simple harmonic oscillators of frequencies (transverse-optic frequencies) ω_{TOi}, dielectric strengths S_i, and damping γ_i:

$$\epsilon(\omega) = \epsilon_\infty \left[1 + \sum_i \frac{S_i \omega_{TOi}^2}{\omega_{TOi}^2 - \omega^2 + i\omega\gamma_i} \right], \tag{5}$$

where i is summed over the number of oscillators and ϵ_∞ is the square of the index of refraction of light. For clarity Eq. (5) is written without any subscripts which indicate crystallographic direction. When the terms $\epsilon(\omega)$ and ϵ_∞ refer to the dielectric constant along the z axis, then the relevant transverse modes are all the $A_1(TO)$ modes, each with damping γ_i and strength S_i. Along the x axis the relevant modes have $E(TO)$ character. This form for $\epsilon(\omega)$ displays the low-frequency clamped dielectric constant:

$$\epsilon(0) = \epsilon_\infty \{1 + \sum S_i\} . \tag{6}$$

The Raman emission $I(\omega)$ is proportional to the imaginary part of the dielectric constant $\epsilon''(\omega)/\omega$. Thus, assuming that one mode ω_{TO} dominates $\epsilon(0)$, the Raman emission intensity is given by[4]

$$I(\omega) \propto \frac{KT\epsilon'(0)\gamma\omega_{TO}^2 P_s^2}{(\omega_{TO}^2 - \omega^2)^2 + \gamma^2\omega^2} , \tag{7}$$

where P_s is the spontaneous polarization, $\epsilon'(\omega)$ is the real part of the dielectric constant, and the high-temperature expansion of the Bose–Einstein factor has been used. Figure 7 shows typical results for intensity vs ω of the lowest $E(1TO)$ mode at two temperatures near T_c. The calculated line is of the form shown in Eq. (7) with a frequency-independent dependent γ. In general, the fit is very good except on the high-frequency side, where the calculated line is more intense than the measured. It is not clear if this difference is significant, or due to the manner in which a base line is chosen. A base line is chosen by determining the frequency where there appears to be no signal. This is extrapolated back to lower frequency. The arbitrariness associated with this method possibly accounts for much of the difference between the calculated and measured values at high frequency. On the low-frequency side the measurements shown in Fig. 7 begin at $\approx 18\ cm^{-1}$, whereas previous ones[17] begin at 20–25 cm^{-1}. More recently, we have used much smaller slits and found that to $\approx 9\ cm^{-1}$ the agreement with the measured and calculated line shape is excellent using the same frequency-independent γ. Thus we conclude that Eq. (5) with a frequency-independent γ fits the experimental results in $PbTiO_3$ for the soft $E(1TO)$ mode from at least ≈ 9–90 cm^{-1}.

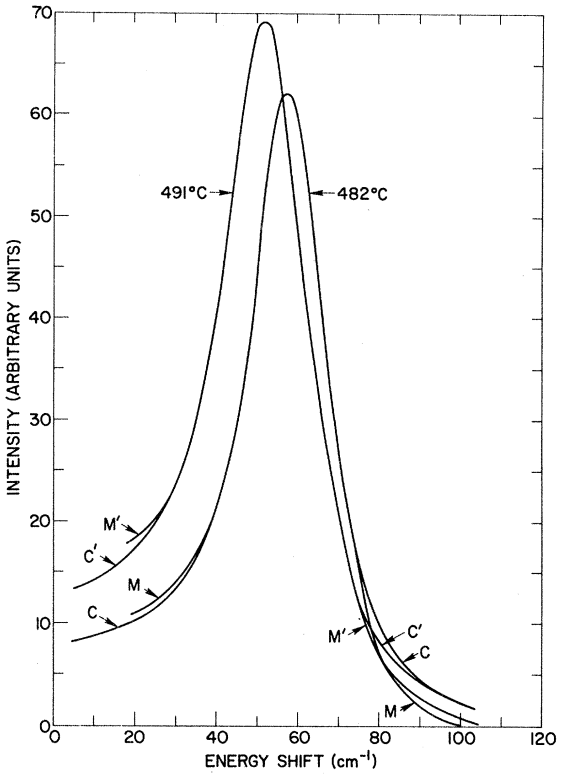

FIG. 7. Experimentally observed (M) and calculated (C) line shapes for the lowest $E(1TO)$ mode at two different temperatures near T_c.

The fit of the experimental data on the resultant ω_{TO} and γ was obtained by trial and error. However, the initial choices for these two parameters were obtained in a simple way and often no adjustments were needed. The frequency corresponding to the peak intensity is ω_p. From Eq. (7), $dI(\omega)/d\omega = 0$ yields

$$\omega_p = \omega_{TO}[1 - \tfrac{1}{2}(\gamma/\omega_{TO})^2]^{1/2} . \tag{8}$$

The ratio of the intensity at the peak, $I(\omega_p)$, to the intensity at zero frequency, $I(0)$, is obtained from Eq. (7):

$$\frac{I(\omega_p)}{I(0)} = \frac{(\omega_{TO}/\gamma)^2}{1 - \frac{1}{4}(\gamma/\omega_{TO})^2} . \tag{9}$$

Equations (8) and (9) are two measurable quantities from which γ and ω_{TO} can be obtained. Table I shows how these results were used. From the measured ratio of the intensities, using Eq. (9), γ/ω_{TO} could be obtained. Then, via Eq. (8), ω_p/ω_{TO} was calculated. From the measured ω_p, both ω_0 and γ were obtained and used as initial choices in Eq. (7) to determine the agreement between calculated and observed $I(\omega)$. Small adjustments in the parameters were sometimes required. Changes in ω_{TO} would affect the calculated results to a much

TABLE I. Values of the quantities contained in Eqs. (8) and (9) used for the calculation of the $E(1TO)$ line shape given by Eq. (7).

γ/ω_0	ω_p/ω_0	$I(\omega_p)/I(0)$
0.05	0.999	400
0.1	0.997	100
0.15	0.994	44.7
0.2	0.989	25.2
0.25	0.984	16.2
0.3	0.977	11.3
0.35	0.968	8.42
0.4	0.959	6.51
0.45	0.948	5.20
0.5	0.935	4.26
0.55	0.921	3.57
0.6	0.905	3.05
0.65	0.888	2.64
0.7	0.868	2.32
0.75	0.847	2.06
0.8	0.824	1.86
0.85	0.799	1.69
0.9	0.771	1.54
0.95	0.740	1.43
1	0.707	1.33

larger extent at $\omega > \omega_p$, and changes in γ would affect the calculated results most strongly at $\omega < \omega_p$. This fitting, normalizing, and plotting procedure was easily accomplished using a time-sharing computer terminal and the conversational language APL (A Programming Language).

Although the basic principles of the effects of anharmonicity on quantities such as $\gamma(\omega)$ are understood,[26] quantitative agreement is seldom obtained[27] even for simple systems. A model for $SrTiO_3$, which includes in a very simple way the anharmonic interactions between normal modes, has been used to calculate the infrared reflectivity.[28] This calculation[28] is in some frequency ranges in better agreement with the data[5(d)] than the classical-oscillator fit,[5(d)] and in other ranges in poorer agreement. Such a comparison to infrared-reflectivity data can be contrasted to a more empirical approach[29] in $SrTiO_3$, where the model used was one in which the low-frequency mode was coupled to the high-frequency mode. A good fit to the reflectivity was obtained.[29]. In the work reported here only a limited frequency range was covered (≈ 9–90 cm^{-1}), but it appears that the simple-damped-harmonic-oscillator form, Eq. (5), fits the data very well.

Recently, neutron spectroscopy[30] disclosed the presence of an anomalous line at zero wave vector in $SrTiO_3$. Silverman[31] has calculated a Raman response at zero frequency that would become observable when the damping becomes comparable to the harmonic frequency. Cowley has also calculated[32] a zero-frequency response in piezoelectric crystals. We have attempted to observe such behavior for the soft $E(1TO)$ mode near T_c. The slits on the monochromator were decreased until the $E(1TO)$ mode was just detectable (signal-to-noise ratio of ≈ 2). The spectrum was measured at several temperature between 450 °C and T_c. For $\omega \geq 4$ cm^{-1} no anomalous behavior could be detected.

V. TEMPERATURE DEPENDENCE

A. Temperature Dependence of the Soft Modes

In this section we compare the temperature dependence of the mode frequencies with other experimental data, namely, spontaneous polarization and spontaneous strain as given by the crystal c/a ratio. We compare the mode frequencies and strengths with those calculated from Devonshire theory and other models.

From mean-field as well as the self-consistent phonon model calculations[33–35] the frequency of the $A_1(1TO)$ mode is expected to be proportional to an order parameter in the ferroelectric phase. The order parameter is the spontaneous polarization P_s for a ferroelectric. However, it should be remarked that this proportionality has not been proved in general. Thus, it is important to establish the relationship between the temperature dependence of $A_1(1TO)$ and P_s. Recent accurate experimental measurements of ΔP_s using pyroelectric techniques show that P_s changes by 39 μC/cm^2 between room temperature and T_c.[22] To fix the absolute scale, P_s was measured at room temperature. However, the reported[22] room-temperature value of 57 μC/cm^2 obtained using a pulsed-field technique and based on a single measurement undoubtedly is much too low. (This would lead to a value of 18 μC/cm^2 at T_c, which is what is found in $BaTiO_3$ at its transition temperature; however, the spontaneous strain in $BaTiO_3$ is 3.3 times smaller.) Conventional hysteresis-loop measurements yield[36] 75 μC/cm^2 at room temperature and 40 μC/cm^2 at T_c. Theoretical estimates range from[37] 54 to 81 μC/cm^2.

Since theory suggests $\omega(A_1(1TO)) \propto P_s$, we have taken the approach of fitting the temperature dependence of the measured $A_1(1TO)$ Raman data with measurements of $P_s = \Delta P_s + P_0$, where $P_0 = P_s(T_c)$ and ΔP_s is taken from the pyroelectric measurements. Figure 8 shows the normalized results for $P_0 = 42$ μC/cm^2. With this value of P_0 the room-temperature value of P_s would be 81 μC/cm^2. The resulting agreement with the experimental results obtained by standard loop measurements[36] is very good.

As another check on the above-determined relationship, $P_s = \Delta P_s + 42$ μC/cm^2, we can compare the $A_1(1TO)$-mode frequencies with the experimen-

tally determined spontaneous strain by means of the relation $P_s^2 \propto (c/a) - 1$. (The constant of proportionality for the $BaTiO_3$ case is found to be the same regardless of the measurement technique.[38]) Figure 8 shows $(c/a-1)^{1/2}$ normalized to 65.8 cm^{-1} at T_c. There is reasonable agreement between the two measurements particularly in the interval ~200 °C below T_c.

The constant of proportionality that relates the strain x_{ij} to the polarization bilinearly, $P_k P_l$, is the electrostrictive coefficient Q_{ijkl}, which is a fourth-rank tensor. For a stress-free crystal such as $PbTiO_3$ in the cubic phase,[38]

$$x_{ij} = Q_{ijkl} P_k P_l , \quad x_3 = Q_{33} P_3^2 , \quad x_1 = Q_{13} P_3^2 , \qquad (10)$$

where we have used the (Voight) contracted notation in the last two equations of Eq. (10). Here, the 3-index refers to the z axis and the 1-index to the x axis. If these electrostrictive coefficients are independent of temperature then values obtained above and below T_c should be in good agreement. This is indeed the case in $BaTiO_3$.[38] From Eq. (10) one can obtain

$$c/a - 1 = (Q_{33} - Q_{13}) P_s^2 . \qquad (11)$$

Using the room-temperature results[39] for c/a and P_s ($= \Delta P_s + 42\ \mu C/cm^2$), as shown in Fig. 8, one obtains $Q_{33} - Q_{13} = 1.1 \times 10^{-12}$ cgs for $PbTiO_3$. It is interesting to note that in $BaTiO_3$,[38] $Q_{33} - Q_{13} = 1.8 \times 10^{-12}$ cgs, which is similar to the lead salt. This indicates the similarity of these two perovskite crystals.

The relation in Eq. (10) could give Q_{33} and Q_{13} separately. However, to determine each quantity separately the deviation of the c axis and a axis from a reference value must be known. In $BaTiO_3$ this reference could be taken as the high-temperature cubic cell constant extrapolated below T_c or as the cube root of the volume.[38] Both approaches yield similar results in $BaTiO_3$.[38] However, this is not true in $PbTiO_3$, where the extrapolated cubic cell constant would yield temperature-dependent individual electrostrictive constants. However, using the cube root of the volume as a reference,[39] we obtain $Q_{33}/Q_{13} = -2$ for $PbTiO_3$, whereas the ratio is -2.2 in $BaTiO_3$. Thus, in this respect, the two salts behave in a similar manner.

For comparison with the A_1(1TO), the soft E(1TO) frequency is also shown in Fig. 8, but normalized to 65.8 cm^{-1} at T_c. Two points are immediately noticeable. First, the E-mode temperature dependence is somewhat flatter than that of the A_1 mode. This is similar to behavior observed[40] in $SrTiO_3$ below the structural phase transition at 110 °K. The flatter temperature dependence of the E mode compared to the A_1 mode is expected from theory.[33,35] Secondly, the E(1TO) mode is approximately proportional to P_s near T_c,

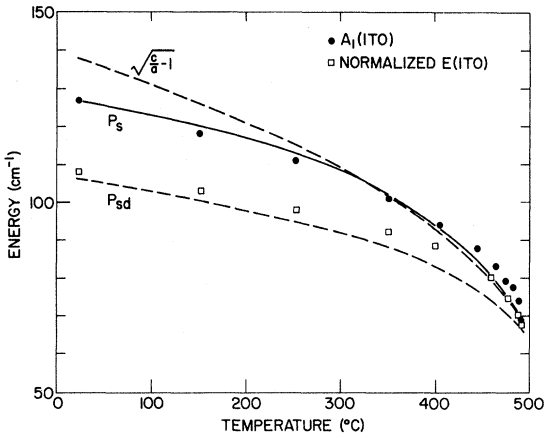

FIG. 8. Frequency of the A_1 (1TO) mode (solid circles) as a function of temperature. The solid curve, P_s, was obtained from experimental pyroelectricity data (Ref. 22) and the value of the spontaneous polarization at T_c was adjusted to have the curve fit the frequency data of the A_1(1TO) mode as discussed in the text. The dashed curve $(c/a-1)^{1/2}$ was obtained assuming the polarization proportional to the spontaneous strain. The curve is normalized at T_c to the A_1(1TO) frequency. Curve P_{sd} was calculated assuming a Devonshire-like dependence of polarization on temperature. All curves are normalized to 65.8 cm^{-1} at T_c. Normalized E(1TO) data are also shown for comparison.

which is also in agreement with theory.[33,35]

The results in Fig. 8 for the temperature dependence of $\omega[A_1(1TO)]$ can be compared to that calculated from the Devonshire free-energy theory. The three-term Devonshire expression for the difference in free energy between the polarized and unpolarized reference phase at constant temperature is[1]

$$F(P, T) - F(0, T) = A(T - T_0)P^2 - BP^4 + CP^6 , \qquad (12)$$

where P is the polarization and A, B, and C are constants, at least over some limited temperature range. From the minima of the free energy $(\partial F/\partial P)_T = 0$, an equation for the temperature dependence of the spontaneous polarization P_{sd} can be obtained[1,41]:

$$P_{sd}^2 = \tfrac{2}{3} P_c^2 [1 + (1 - \tfrac{3}{4}\tau)^{1/2}] , \qquad (13)$$

$$P_c^2 = B/2C , \quad \tau = (T - T_0)/(T_c - T_0) . \qquad (14)$$

P_c is the spontaneous polarization at T_c, and τ is a dimensionless temperature factor. Taking $T_c - T_0 = 42$ °C from a recent measurement,[22] no parameters are required other than normalization at T_c. Figure 8 shows the result calculated from Eq. (13). The curve is normalized at T_c to 65.8 cm^{-1}. The Devonshire P_{sd} is below P_s and $\omega(A_1(1TO))$ over the entire temperature range shown. The free-energy expression, Eq. (12), contains only three

terms, which are close in value. [For example, at $T=T_c$, P_c is given in Eq. (14) and[1,41] $A(T_c-T_0)=B^2/4C$, so the three terms on the right side of Eq. (12) are in the ratio $1:-2:1$.] In $BaTiO_3$[42] this limited expansion of the free energy shows up clearly in a very strong temperature dependence of the B coefficient of Eq. (12). Thus we conclude that good agreement between the theoretical Devonshire spontaneous polarization P_{sd} and the experimental value, or the value of $\omega[A_1(1\text{TO})]$, should not be expected over a large range of temperature.

B. Temperature Dependence of the Mode Strengths

Measurements of the mode dielectric strengths are of considerable importance as they permit an unambiguous determination of $\epsilon(0)$, the clamped zero-frequency dielectric constant. In this manner the mode(s) responsible for the dielectric behavior of the $PbTiO_3$ can be ascertained and compared with $BaTiO_3$.[12] The dielectric strengths S_i of the modes, as in Eqs. (5) and (6), can be determined from knowledge of the transverse and longitudinal frequencies. The longitudinal frequencies are given by the zeros of the dielectric constant, $\epsilon(\omega_{LO})=0$. If all ω_{TO} and ω_{LO} are known, then for the three A_1 modes the requisite S_i values can be obtained from three simultaneous equations. Similar considerations apply to the three E modes. Table II collects our results for $PbTiO_3$, as well as those reported[5(d),12] in $BaTiO_3$ for comparison. Figure 9 shows the temperature dependence of S_i for the three A_1 modes and the three E modes.

Consider first the A_1 modes. As demonstrated in Table II and Fig. 9, the lowest $A_1(\text{TO})$ mode exhibits the largest dielectric strength at all temperatures. Thus, it is this mode which dominates the dielectric behavior along the ferroelectric c axis at all temperatures below T_c. Only in $BaTiO_3$ are comparable measurements available at room temperature, where it was unexpectedly found that the middle A_1 mode, $A_1(2\text{TO})$ (at 270 cm^{-1}), dominates the dielectric constant along the c axis[12] (cf.

TABLE II. Frequencies and dielectric strengths of the A_1 and E LO and TO modes of $PbTiO_3$ and $BaTiO_3$ [Refs. 5(d) and 12].

A_1 modes					
	$PbTiO_3$			$BaTiO_3$	
$A_1(\text{TO})$ (cm^{-1})	$A_1(\text{LO})$ (cm^{-1})	S_i	$A_1(\text{TO})$ (cm^{-1})	$A_1(\text{LO})$ (cm^{-1})	S_i
127	215	4.46	170	185	0.44
364	445	0.63	270	475	4.24
651	797	0.36	520	725	0.20
E modes					
	$PbTiO_3$			$BaTiO_3$	
$E(\text{TO})$ (cm^{-1})	$E(\text{LO})$ (cm^{-1})	S_i	$E(\text{TO})$ (cm^{-1})	$E(\text{LO})$ (cm^{-1})	S_i
89	128	10.11	34	180	362
221	445	5.37	183	460	0.44
508	717	0.27	500	700	0.16

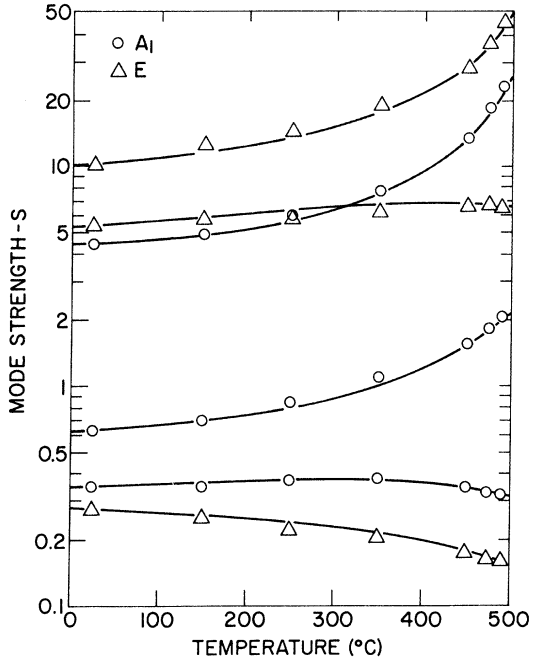

FIG. 9. Temperature dependence of three A_1- and three E-mode dielectric strengths.

Table II). On the other hand, from Table II it is clear that $PbTiO_3$ has the behavior expected,[1,3] since the lowest A_1 mode at all temperatures in the ferroelectric phase dominates $\epsilon(0)$ along the ferroelectric c axis. Figure 10 shows a plot of $\epsilon(0)=\epsilon_\infty(1+\sum S_i)$ along the a and c axes [Eq. (6)], with[42] ϵ_∞ estimated to be $(2.52)^2=6.37$. Note that S_i, as written in Eqs. (5) and (6), is independent of ϵ_∞.

We have attempted to fit the clamped dielectric constant ϵ along the ferroelectric c axis using the Devonshire free-energy formulation of Eq. (12). For large ϵ, $4\pi/\epsilon=(\partial^2F/\partial P^2)_T$, and ϵ along the c axis becomes

$$\epsilon_{cd}=G[(1-\tfrac{3}{4}\tau)+(1-\tfrac{3}{4}\tau)^{1/2}]^{-1/2}, \tag{15}$$

$$G=3\pi[8A(T_c-T_0)]^{-1}, \tag{16}$$

where τ is defined in Eq. (14). In Fig. 10 a plot of ϵ_{cd} is shown taking G as a free parameter to give a least-squares fit to the data. The fit obtained in Fig. 10 is quite poor although the general temperature dependence of the data is followed. However, a value of $G=232$ was required to obtain the curve in Fig. 10, whereas $G=1200$ would be calculated from Eq. (16) using experimental measurements[22] of A, T_c, and T_0 obtained from dielectric data above T_c.

In view of the poor fit of the Devonshire clamped $\epsilon(0)$ to our experimental temperature dependence, we have modeled the dielectric data along both axes to an empirical equation of the form

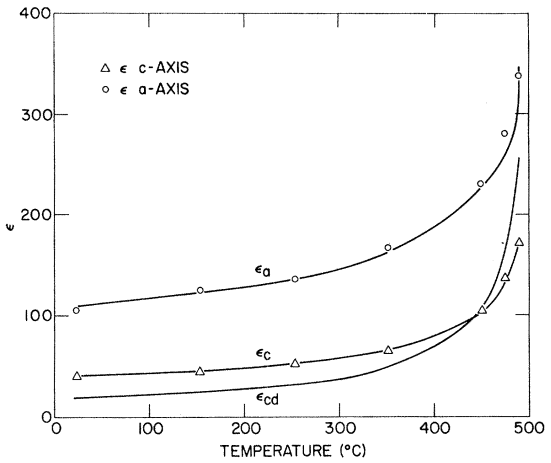

FIG. 10. The experimental clamped dc dielectric constants of $PbTiO_3$ along the a and c axes calculated from the temperature dependences of the A_1- and E-mode dielectric strengths. The solid curve through the data points is a fit from Eqs. (17) and (18). For comparison, the clamped c-axis dielectric constant at zero frequency has been calculated from the Devonshire formulation (ϵ_{cd}).

$$\epsilon = G(T_u - T)^n , \tag{17}$$

$$T_u = T_0 + \tfrac{4}{3}(T_c - T_0) . \tag{18}$$

The form of Eq. (17) has its origin in the fact that the dielectric constant of Eq. (15) diverges upon heating at a temperature T_u, above T_c, given by Eq. (18). This is rigorous if one ignores the adiabatic correction, a reasonable approximation for the perovskites. Taking[22] $T_c = 493$ °C and $T_0 = 450$ °C, we obtain $T_u = 507$ °C. It is clear from Fig. 10 that the empirical equation fits the data very well over a very large temperature range. The two parameters, obtained by a least-squares fit, are $G = 674$ and 966, $n = -0.447$ and -0.340, for ϵ along the c axis and a axis, respectively.

For the E modes the lowest mode in $PbTiO_3$ has the largest strength at room temperature. Moreover, as T_c is approached its strength becomes fractionally more important since the strength of the next lowest mode is essentially independent of temperature (Fig. 9). In $BaTiO_3$ the lowest E mode has all the dielectric strength at room temperature. Of course in $BaTiO_3$ this very-low-frequency (34 cm^{-1}) E mode, with very large S_i, is associated with the transition below room temperature to the orthorhombic form.[1]

C. Temperature Dependence of the Damping Constant

As discussed in Sec. IV and Ref. 17, the shape of the lowest E(TO) mode, E(1TO), can be fit very well by a function of the form of Eq. (7) which is based on a damped-harmonic-oscillator model. The details of the temperature dependence of γ are given in Ref. 17. Some of the measurements just below T_c were taken at 0.25 °C intervals and Eq. (7) fits the line very well to the temperature at which the line disappeared.

In Ref. 17, γ vs temperature was fit to a functional form obtained from the Devonshire dielectric constant along the c axis. (Recall that the E modes determine the dielectric constant along the a axis.) However, it was also pointed out that the fit is not unique, since we could find other fits to the data. The empirical form of Eq. (17) also can be used to fit the temperature dependence of γ very well. Table III shows the results for two temperature intervals. We take the smaller interval near T_c with the thought that the changes in the order parameter are largest in this region. Thus, this region probably represents the ferroelectric effects with little interference from normal thermal effects that certainly enter into the larger range of 23 °C to T_c. As can be seen in Table III, the empirical equation fits very well in both temperature intervals.

We have also used the same form, Eq. (17), to fit the soft-E- and soft-A_1-mode frequencies. As can be seen in Table III, the fit is also good. However, we emphasize again that no theoretical justification exists for this functional form. In fact, for the mode frequencies, there are theoretical calculations showing that for $T = T_u$ the frequencies are not zero for a first-order transition.[43] This will be discussed in Sec. V D.

Examining the empirically fit curves for the mode frequencies, for the E(1TO) mode between 460 °C and T_c we find $\gamma[\omega(E(1\mathrm{TO}))]^2 = \text{const}$. At any temperature in this interval the value of $\gamma\omega^2$ is

TABLE III. Parameters of the empirical fits to the A_1(1TO) and E(1TO) frequencies and E(1TO) damping constant for a wide and a narrow temperature interval up to T_c. The empirical function is given in Eqs. (17) and (18). The numbers in parentheses are the minimum deviations, Eq. (25).

Temperature range (°C)	γ G (cm^{-1})	n	E(1TO) G (cm^{-1})	n	A_1(1TO) G (cm^{-1})	n
$23 \le T \le T_c$	81.5	−0.397	38.7	0.135	42.9	0.172
	(0.861)		(0.593)		(1.543)	
$460 \le T \le T_c$	63.2	−0.317	36.1	0.157	42.0	0.180
	(0.207)		(0.351)		(1.481)	

at most 5% larger than its value at T_c. For the larger temperature interval, 23 °C to T_c, $\gamma\omega^2$ is reasonably constant by fitting the values at lower temperatures. However, this fit is not very good for $T \geq 460$ °C since deviations from the value at T_c of up to 23% are obtained. Figure 11 shows the experimental results between 400 °C and T_c and the least-squares fits from Table III in the 460 °C to T_c interval. As will be discussed in the second paper in this series, the singular behavior for γ is observed in a wide range of solid-solution perovskite ferroelectrics for the soft E mode, but not the lowest A_1 mode. This is observed as long as the soft E mode is not too highly damped. In pure $BaTiO_3$, where the damping is larger than the harmonic frequency of the E mode, γ appears to have at most only a small temperature dependence. Silverman[31] has proposed a theory for the temperature dependence of the damping constant.

D. Comment on Critical Effects

In this section we examine the possible role of critical effects in influencing the soft-mode TO frequency near the first-order transition in $PbTiO_3$. Such effects have been reported at the first-order transition in quartz.[44]

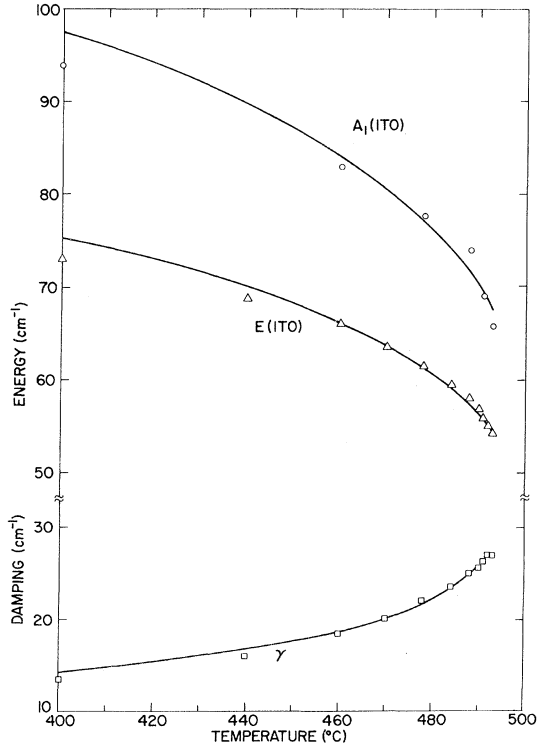

FIG. 11. Experimental values of the A_1(1TO)- and E(1TO)-mode frequencies and the E(1TO) damping constant compared with calculated results based on an empirical model discussed in the text (solid curves).

Figure 12 shows the free-energy curve for several temperatures near a first-order transition at a temperature T_c. T_u is the superheating temperature, above which there is no longer a zero for $d\Delta F/dP$ except at $P=0$. If there were no thermal effects the system would stay ordered for temperatures above T_c until T_u was reached. At T_u there is no longer a minimum in ΔF except at $P=0$, so the system no longer has a polarization. The value of the order parameter P corresponding to approaching T_u from below is called P_u. Figure 12 also shows P vs temperature. In the lower curve, at T_u, dP/dT diverges. Also shown on the P-vs-T curve is the temperature T_0 which is the supercooling temperature, corresponding to the temperature below which there is no longer a local minimum at $P=0$, as also shown in the ΔF-vs-P plot.

The Devonshire free energy,[1] Eq. (12), can be used to determine P_u and T_u in terms of measurable quantities. The result is

$$P_u = P_c(\tfrac{2}{3})^{1/2}, \quad T_u = T_0 + \tfrac{4}{3}(T_c - T_0). \tag{19}$$

The result for T_u already has been given in Eq. (18) since this is also the divergence temperature of the dielectric constant in the ferroelectric phase. Writing the temperature dependence of the polarization in terms of P_u and T_u we obtain

$$P = P_u \left\{1 + \left[\frac{3}{4}\,\frac{T_u - T}{T_c - T_0}\right]^{1/2}\right\}^{1/2}. \tag{20}$$

Expanding for $T_u - T < \frac{4}{3}(T_c - T_u)$, we obtain

$$P = P_u + \tfrac{1}{4}\sqrt{3}\,P_u\left(\frac{T_u - T}{T_c - T_0}\right)^{1/2} + \cdots. \tag{21}$$

If critical effects are important an exponent in the temperature term of $\frac{1}{3}$ might be expected.[44] To compare these results to the experimental results we need only assume that the soft-mode frequency is proportional to the order parameter. As previously discussed, this is a result that all theoretical models predict, although it has not been shown to be true in general. Thus, assuming only that $\omega \propto P$, $\omega_u = (\frac{2}{3})^{1/2}\omega_c$ from Eq. (21), and taking the relation for T_u from Eq. (18), we obtain

$$\omega = \omega_u + K(T_u - T)^{1/2} + \cdots, \tag{22a}$$

$$K = \tfrac{1}{4}\sqrt{3}\,\frac{\omega_u}{(T_c - T_0)^{1/2}}. \tag{22b}$$

Again, critical effects would suggest a $\frac{1}{3}$ for the exponent of the temperature dependence in Eq. (22a), instead of $\frac{1}{2}$ as found from Devonshire's free-energy expression.

We have used Eq. (22a) to fit the experimental temperature dependence of the soft-mode frequencies. The first consideration in fitting is the temperature range that should be used. We already have seen in Fig. 8 and the discussion in Sec. V A

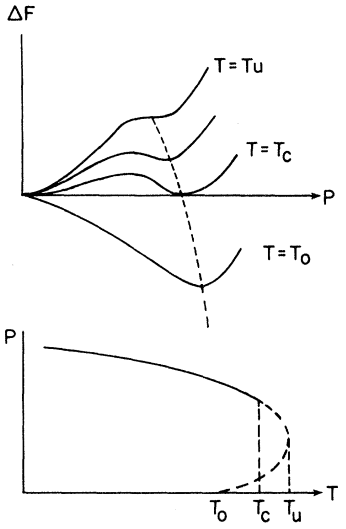

FIG. 12. Free-energy and polarization curves for temperatures near a first-order transition at T_c [after Devonshire (Ref. 1)].

that the Devonshire form for the spontaneous polarization does not fit the temperature dependence of the soft A_1 mode over the temperature interval 23 °C to T_c. On the other hand, it is apparent that very near T_c a straight line could be used to fit the data. We have taken the approach of rewriting Eq. (22a) as a two-parameter equation to be least-squares fit to the experimental data over several ranges of temperature. Fixing $T_u = 504$ °C and $\omega_u = 53.7$ cm^{-1} for the A_1(TO) mode from Eq. (19), we rewrite Eq. (22) in the form

$$\omega = \omega_u + \alpha(T_u - T)^{\beta}, \tag{23}$$

where α and β are determined from a least-squares fit to the experimental data. For example, in the temperature interval 445 °C to T_c, we obtain $\alpha = 2.87$ and $\beta = 0.621$. This temperature interval is probably close to the largest that can be used in the expansion of Eq. (19) to the form contained in (20). On the other hand, for the temperature interval 400 °C to T_c we obtain, for a fit to the A_1-mode data, $\alpha = 3.68$ and $\beta = 0.541$. For larger temperature intervals the values of α and β do not vary significantly. (For example, in the interval 350 °C to T_c, $\alpha = 4.22$ and $\beta = 0.497$.) From the expansion of Devonshire's equations, Eq. (21), we would predict $\alpha = 3.55$ and $\beta = \frac{1}{2}$. Thus, we are forced to conclude that we have not seen critical effects in the temperature dependence of the soft A_1(TO) mode. Also, to the extent that we can determine the curvature of the A_1(1TO)-mode frequency with temperature, an expansion of Devonshire's equations is in modest agreement with the experimental results near T_c.

To be able to compare our approach more directly to work describing the critical effects at the first-order transition in quartz[44] we attempted a four-parameter fit. Thus, we used Eq. (23) for a least-squares fit of the soft A_1(TO) data, but allowed all four parameters ω_u, T_u, α, and β to vary as was done for quartz.[44] With four parameters we find that the experimental data can be fit very well with a large variety of exponents β. For example,

$$\begin{aligned} \omega &= 55 + 9.06\,(495.25 - T)^{0.332}, \\ \omega &= 35 + 27.22\,(495.25 - T)^{0.170}. \end{aligned} \tag{24}$$

Both fit the experimental data to within no more than 2 cm^{-1} disagreement, which is better than the experimental accuracy of the frequency measurement for these wide lines. Defining the minimum deviation as

$$\left[\sum_{i=1}^{N} (\omega_{\mathrm{calc}_i} - \omega_{\mathrm{meas}_i})^2\right] \Big/ N, \tag{25}$$

the minimum deviations for the two fits of Eq. (23) are 1.59 and 0.86, respectively. Therefore, we conclude that the parameters in the four-parameter fits are not significant owing to the fact that for a large variety of parameters and exponents, the experimental data can be fit within its limits of error.

These results are significant with respect to the use of many-parameter fits in interpreting experimental data. Considering further the quartz elastic constant data,[44] we find that a large number of fits to the experimental elastic constant data are possible. We have found, for example, that exponents, β in Eq. (23), may range from the reported 0.34 to as low as 0.2. Moreover, the least-squares deviation, Eq. (24), is a factor more than 2 smaller for the latter value of β than for the 0.34 value. However, both calculated curves, for the elastic constants, fit the data to what is probably better than the experimental accuracy. From these results it appears to the present authors that as yet there is in fact no experimental evidence from Raman measurements for critical effects at first-order transitions. Finally, it is also evident that a four-parameter fit of the type in Eq. (23) requires very accurate experimental data before the coefficients can be trusted to have physical meaning. We would expect that a two-parameter fit is more realistic provided that the values of ω_u and T_u are separately determined.

VI. ADDITIONAL COMMENTS

Axe[45] has shown that with a knowledge of the parameters in Eq. (5), the atomic displacements in the ferroelectric phase, and several other reasonable assumptions, it is possible to calculate the spontaneous polarization. We calculated the room-temperature polarization of $PbTiO_3$ using the

frequency and strength of the lowest A_1 mode from Table II, the published atomic displacements,[46] and the treatment given in Ref. 25. The result obtained is $P_s = 55\ \mu C/cm^2$. This value is somewhat lower than the value 81 $\mu C/cm^2$ found in Sec. V A, or that determined from hysteresis loops[36] (75 $\mu C/cm^2$). However, in view of the assumptions made, it is in modest agreement with the results. The calculation[45] assumes that the eigenvector of the lowest and most important normal mode does not vary with temperature. The temperature dependence of the effective charge of the lowest A_1 mode was calculated in $PbTiO_3$ to test the validity of this assumption. The effective charge is proportional to $S_i\omega_{TOi}^2$, as can be seen from Eq. (5). Using the data for A_1(1TO) from Figs. 4 and 9, it is found that a variation of 0.7 to 1.0 is obtained between room temperature and T_c. This percentage variation of the effective charge of the lowest A_1 mode, although not large, is certainly indicative that the eigenvectors of the A_1 modes cannot be treated as completely independent of temperature.

The mode-frequency results reported here can be compared to a less complete study[20] of $PbTiO_3$ using unpolarized Raman measurements and polarized infrared techniques. The infrared-reflectivity measurements for the E modes seem to show[20] some extra features, but with the use of a Kramers–Kronig (KK) analysis three transverse modes at 115, 255 and 510 cm^{-1} were obtained. (Reflectivity and KK results are in Fig. 1 of Ref. 21.) These compare to the room-temperature values obtained in the present study of E(TO) of 89, 221, and 508 cm^{-1}. For the longitudinal modes the KK analysis gave[20] 135, 445, and 680 cm^{-1} while the values obtained here for E(LO) are 128, 445, and 717 cm^{-1}. As can be seen, the agreement in some cases is very good, but in others, quite poor. It is more difficult to compare the data presented here to the infrared A_1-mode data (Fig. 2 of Ref. 20) because of the large number of extra features obtained from the reflectivity data. If the principal features from the KK analysis are used, the agreement between the infrared data and the Raman results reported here for the A_1 modes is poor (only two out of the six modes agree). This poor agreement is probably related to the extra features in the reflectivity data. We also note that the temperature dependence of the KK analysis for the lowest mode above T_c does not appear to obey a $(T - T_c)^{1/2}$ law as expected from the Curie-Weiss behavior[22] of ϵ and the Lyddane–Sachs–Teller relationship.

The results determined from unpolarized Raman measurements[20] of course cannot be uniquely assigned as to mode type, A_1 or E, and TO or LO. Actually, the data obtained (Fig. 5 of Ref. 20) appear to look rather similar to the results of powder Raman measurements.[25] This is probably fortunate since there can be a number of strong, sharp quasimodes which would appear if a single crystal with several arbitrary orientations were used. However, a crystal with a very large number of arbitrary orientations would be similar to a powder so that the quasimodes get averaged and powder Raman results apply.[25] The temperature dependences of the unpolarized results,[20] in general, are similar to the polarized results reported here (see Fig. 4) except that the unpolarized modes cannot definitely be assigned.

The very interesting questions remain as to why $PbTiO_3$ is well behaved, in that the Raman selection rules are obeyed up to and above T_c, and the modes underdamped to T_c. We have no clear answers for these two questions and can only speculate at this time. Silverman[31] has shown that it is possible to explain the divergence of the damping constant γ by relating the temperature-dependent frequency of the mode to the separation of, for example, the transverse- and longitudinal-acoustic branches. This type of coincidence could also account for the highly overdamped mode in $BaTiO_3$.[4(c),4(d)] Possibly the selection-rule problem in $BaTiO_3$,[4] and lack of one in $PbTiO_3$, is closely related to line-broadening effects in the sense they are both related to strong anharmonic effects and/or separations of branches in the Brillouin zone. One noticeable difference between $BaTiO_3$ and $PbTiO_3$ is that the latter contains a much more rigid oxygen octahedron[46] in the ferroelectric phase. Since the short-range forces between the oxygen atoms are large, the approximate "cubic" symmetry in $PbTiO_3$ could reduce the anharmonic forces. In ferroelectric $BaTiO_3$ the oxygen octahedra is distorted so these forces could be larger.

It also should be pointed out that if $BaTiO_3$ is disordered above and/or below T_c as suggested,[7,47] the differences between $BaTiO_3$ and $PbTiO_3$ could be due to factors remote from those considered above. However, the diffuse x-ray results[7] leading to a disorder model of $BaTiO_3$ have been explained in other ways,[15,48] so that there is as yet no apparent approach to resolving the problem.[49]

ACKNOWLEDGMENTS

We wish to thank F. Dacol and K. H. Nichols for the expert experimental assistance throughout all phases of this work. Also, it is a pleasure to acknowledge discussions with Professor E. Burstein, Dr. E. Pytte, Dr. N. S. Shiren, and Dr. B. D. Silverman.

†Partially supported by the Army Research Office, Durham, N. C.

[1](a) F. Jona and G. Shirane, *Ferroelectric Crystals* (MacMillan, New York, 1962); (b) E. Fattuzzo and W. J.

Merz, *Ferroelectricity* (Wiley, New York, 1967); (c) W. Kaenzig, in *Solid State Physics* (Academic, New York, 1957), Vol. 4, pp. 1–197.

[2]For example, see, IEEE Trans. Electron Devices **ED-16**, 505 (1969); IEEE Trans. Sonics Ultrason. **SU-19** 67 (1972); Ferroelectrics **3**, 67 (1972).

[3]W. Cochran, Phys. Rev. Lett. **3**, 412 (1959); Adv. Phys. **9**, 387 (1960); Adv. Phys. **10**, 401 (1961).

[4](a) J. L. Parsons and L. Rimai, Solid State Commun. 5, 423 (1967); L. Rimai, J. L. Parsons, J. T. Hickmott, and T. Nakamura, Phys. Rev. **168**, 623 (1968); (b) A. Pinczuk, W. T. Taylor, E. Burstein, and I. Lefkowitz, Solid State Commun. 5, 429 (1967); (c) M. DiDomenico, Jr., S.P.S. Porto, and S. H. Wemple, Phys. Rev. Lett. **19**, 855 (1967); (d) M. DiDomenico, Jr., S. H. Wemple, S. P. S. Porto, and R. P. Bauman, Phys. Rev. **174**, 522 (1968).

[5](a) J. T. Last, Phys. Rev. **105**, 1740 (1957); (b) W. G. Spitzer, R. C. Miller, D. A. Kleinman, and L. E. Howarth, Phys. Rev. **126**, 1710 (1062); (c) J. M. Ballantyne, Phys. Rev. **136**, A249 (1964); (d) A. S. Barker, Jr., Phys. Rev. **145**, 391 (1966).

[6]G. Shirane, B. C. Frazer, V. J. Minkiewicz, J. A. Leake, and A. Linz, Phys. Rev. Lett. **19**, 324 (1967); Y. Yamada, G. Shirane, and A. Linz, Phys. Rev. **177**, 848 (1969).

[7]R. Comes, M. Lambert, and A. Guinier, Solid State Commun. **6**, 715 (1968); Solid State Commun. **7**, 305 (1969).

[8]A. S. Barker, Jr. and M. Tinkham, Phys. Rev. **125**, 1527 (1962).

[9]R. A. Cowley, Phys. Rev. Lett. **9**, 159 (1962); Phys. Rev. A **134**, A981 (1964).

[10]C. H. Perry and T. F. McNelly, Phys. Rev. **154**, 456 (1967).

[11]G. Shirane, R. Nathans, and V. J. Minkiewicz, Phys. Rev. **157**, 396 (1967).

[12]A. Pinczuk, E. Burstein, and S. Ushioda, Solid State Commun. **7**, 139 (1969).

[13]G. Burns and B. A. Scott, Solid State Commun. **9**, 813 (1971).

[14]G. Shirane, J. D. Axe, J. Harada, and A. Linz, Phys. Rev. B **2**, 3651 (1970); J. Harada, J. D. Axe, and G. Shirane, Phys. Rev. B **4**, 155 (1971).

[15]A. Hüller, Solid State Commun. **7**, 589 (1969); Z. Phys. **220**, 145 (1969).

[16]G. Burns and B. A. Scott (unpublished).

[17]G. Burns and B. A. Scott, Phys. Rev. Lett. **25**, 167 (1970).

[18]G. Shirane, J. D. Axe, J. Harada, and J. P. Remeika, Phys. Rev. B **2**, 155 (1970).

[19]R. Loudon, Adv. Phys. **13**, 423 (1964).

[20]C. H. Perry and N. E. Tornberg, in *Light Scattering Spectra in Solids*, edited by G. B. Wright (Springer-Verlag, New York, 1969), p. 467; Phys. Rev. **183**, 595 (1969); N. E. Tornberg and C. H. Perry, J. Chem. Phys. **53**, 2946 (1970).

[21]M. L. Sholokhovich, Zh. Neorg. Khim. **3**, 1214 (1958) [Russ. J. Inorg. Chem. **3**, 207 (1958)].

[22]J. P. Remeika and A. M. Glass, Mater. Res. Bull. **5**, 37 (1970).

[23]L. Merten, Phys. Status Solidi **25**, 125 (1968); Z. Naturforsch. A **22**, 329 (1967).

[24]T. Kurosawa, J. Phys. Soc. Jap. **16**, 1298 (1961).

[25]G. Burns and B. A. Scott, Phys. Rev. Lett. **25**, 1191 (1970).

[26]M. Born and K. Huang, *Dynamical Theory of Crystal Lattices* (Clarendon, Oxford, England, 1954), Secs. 46–48.

[27]R. A. Cowley, Rep. Prog. Phys. **31**, 123 (1968).

[28]R. A. Cowley, Philos. Mag. **11**, 673 (1965).

[29]A. S. Baker and J. J. Hopfield, Phys. Rev. 135, A1732 (1964).

[30]T. Riste, E. J. Samuelsen, K. Otnes, and J. Feder, Solid State Commun. **9**, 1455 (1971).

[31]B. D. Silverman, Solid State Commun. **10**, 311 (1972).

[32]R. A. Cowley, J. Phys. Soc. Jap. Suppl. **28**, 239 (1970).

[33]J. Feder and E. Pytte, Phys. Rev. B **1**, 4803 (1970).

[34]N. S. Gillis and T. R. Koehler, Phys. Rev. B **5**, 1925 (1972).

[35]E. Pytte, Phys. Rev. B **5**, 3758 (1972).

[36]V. G. Gavrilyachenko, R. I. Spinko, M. A. Martynenko, and E. G. Fesenko, Fiz. Tverd. Tela **12**, 1532 (1970) [Sov. Phys.-Solid State **12**, 1203 (1970)].

[37]See Ref. 1(c); Y. N. Venevtser, G. S. Zhadanov, S. P. Soloven, and V. V. Ivanova, Kristallografiya **4**, 255 (1959) [Sov. Phys.-Crystallogr. **4**, 235 (1960)]; R. Machet, J. Boulillot, and L. Godefroy, J. Phys. Soc. Jap. Suppl. **28**, 366 (1970).

[38]See Ref. 1(a), pp. 144–147. We note that Eq. (10) is written $x_3 = Q_{11}P_3^2$ and $x_1 = Q_{12}P_3^2$ in Ref. 1(a) because the values are referred to the cubic phase, where $Q_{11} = Q_{33}$, etc., and $Q_{12} = Q_{13}$, etc. However, we have chosen to write the equation properly in the tetragonal phase. For $BaTiO_3$ the coefficients obtained in both phases are the same.

[39]G. Shirane and S. Hoshino, J. Phys. Soc. Jap. **6**, 265 (1951).

[40]P. A. Fleury, J. F. Scott, and J. M. Worlock, Phys. Rev. Lett. **21**, 16 (1968).

[41]S. Triebwasser, Phys. Rev. **101**, 993 (1956).

[42]M. Drougard, R. Landauer, and D. Young, Phys. Rev. **98**, 1013 (1955); S. Singh, J. P. Remeika, and J. R. Potopowicz, Appl. Phys. Lett. **20**, 135 (1972).

[43]E. Pytte, Solid State Commun. 11, 161 (1972).

[44]U. T. Höchli and J. F. Scott, Phys. Rev. Lett. **26**, 1627 (1971).

[45]J. D. Axe, Solid State Commun. **5**, 413 (1967).

[46]See Ref. 1(a), Fig. V-15 on p. 238 and the references to the x-ray work quoted there.

[47]M. P. Fontana and M. Lambert, Solid State Commun. **10**, 1 (1972).

[48]A. C. Nunes, J. D. Axe, and G. Shirane, Ferroelectrics **2**, 291 (1971).

[49]*Note added in proof.* See also G. Burns, Phys. Letters (to be published).